Ecological Applications, 21(5), 2011, pp. 1573–1590

Simulating fire regimes in the Amazon in response to climate change and deforestation

Rafaella Almeida Silvestrini,[1,5] Britaldo Silveira Soares-Filho,[1] Daniel Nepstad,[2] Michael Coe,[3] Hermann Rodrigues,[1] and Renato Assunção[4]

[1]*Centro de Sensoriamento Remoto, Universidade Federal de Minas Gerais, Avenida Antônio Carlos, 6627, Belo Horizonte, Minas Gerais 31270-900 Brazil*
[2]*Instituto de Pesquisa Ambiental da Amazônia. Avenida Nazaré 669, Belém, Pará 66035-170 Brazil*
[3]*Woods Hole Research Center, 149 Woods Hole Road, Falmouth, Massachusetts 02540-1644 USA*
[4]*Departamento de Estatística, Universidade Federal de Minas Gerais, Avenida Antônio Carlos 6627, Belo Horizonte, Minas Gerais 31270-900 Brazil*

Abstract. Fires in tropical forests release globally significant amounts of carbon to the atmosphere and may increase in importance as a result of climate change. Despite the striking impacts of fire on tropical ecosystems, the paucity of robust spatial models of forest fire still hampers our ability to simulate tropical forest fire regimes today and in the future. Here we present a probabilistic model of human-induced fire occurrence for the Amazon that integrates the effects of a series of anthropogenic factors with climatic conditions described by vapor pressure deficit. The model was calibrated using NOAA-12 night satellite hot pixels for 2003 and validated for the years 2002, 2004, and 2005. Assessment of the fire risk map yielded fitness values >85% for all months from 2002 to 2005. Simulated fires exhibited high overlap with NOAA-12 hot pixels regarding both spatial and temporal distributions, showing a spatial fit of 50% within a radius of 11 km and a maximum yearly frequency deviation of 15%. We applied this model to simulate fire regimes in the Amazon until 2050 using IPCC's A2 scenario climate data from the Hadley Centre model and a business-as-usual (BAU) scenario of deforestation and road expansion from SimAmazonia. Results show that the combination of these scenarios may double forest fire occurrence outside protected areas (PAs) in years of extreme drought, expanding the risk of fire even to the northwestern Amazon by midcentury. In particular, forest fires may increase substantially across southern and southwestern Amazon, especially along the highways slated for paving and in agricultural zones. Committed emissions from Amazon forest fires and deforestation under a scenario of global warming and uncurbed deforestation may amount to 21 ± 4 Pg of carbon by 2050. BAU deforestation may increase fires occurrence outside PAs by 19% over the next four decades, while climate change alone may account for a 12% increase. In turn, the combination of climate change and deforestation would boost fire occurrence outside PAs by half during this period. Our modeling results, therefore, confirm the synergy between the two Ds of REDD (Reducing Emissions from Deforestation and Forest Degradation in Developing Countries).

Key words: *carbon emissions; hot pixels; IPCC A2 scenario; REDD; SimAmazonia.*

Introduction

Human-induced fires play a major role in the dynamics of Amazon forests. Widespread fires burned ~40 thousand km^2 of Amazon forests during the 1997–1998 ENSO (El Niño-Southern Oscillation) event (Nepstad et al. 1999*b*, Alencar et al. 2006). The advent of anthropogenically driven climate change predicts even more human-induced fires not only because of predicted longer dry seasons in some forest regions (Nobre et al. 1991, Malhi et al. 2008), but also due to the reduction of the intervals between extreme drought events (Cox et al. 2004, Marengo et al. 2008). Aside from immediate disturbance effects that can cause a loss of up to 30% of the ecosystem's original complement of species (Slik et al. 2002), the negative consequences of a fire may last for many years. Tree mortality continues for at least two years (Holdsworth and Uhl 1997), and even after 15 years, forests have not regained lost species (Slik et al. 2002). Thus, modeling fire occurrence in the Amazon can be a key approach to assess the effects of the interaction between climate and land use on fire regimes, and thereby to mitigate their potential impacts.

Forest fires also influence global warming. Alencar et al. (2006) estimated that annual committed carbon emissions from fires in the Brazilian Amazon may amount to 0.094 ± 0.070 Pg (1 Pg = 10^9 tons) in ENSO years. However, this figure can be far surpassed in extreme El Niño years, such as the event of 1997–1998, when emissions from forest fires in Mexico, the Amazon,

Manuscript received 27 April 2010; revised 23 November 2010; accepted 6 December 2010. Corresponding Editor: X. Xiao.

[5] E-mail: rafaella@csr.ufmg.br

and Indonesia totaled 1.6 Pg of carbon (Cairns et al. 2000, Phulpin et al. 2002, Page et al. 2003), the equivalent of 18% of current fossil fuel emissions worldwide (JRC 2009). Not only do forest fires alter atmospheric composition, they also interrupt rain cloud formation (Ackerman et al. 2000), thereby reducing rainfall (Andreae et al. 2004) and increasing the average residence time of aerosols in the atmosphere (Ramanathan et al. 2001). These effects also have a significant negative impact on human health (Mendonça et al. 2004). For example, during the extreme drought that affected southwestern Amazon in 2005 (probably associated with the abnormal warming of the tropical North Atlantic [Marengo et al. 2008]), over 40 thousand people in the State of Acre sought medical care due to a persistent smoke plume, which stemmed from multiple fires that burned 300 000 ha of forest in that region (Brown et al. 2006, Aragão et al. 2007).

During Pre-Columbian times, widespread fire events affected the Amazon forest at intervals of 400–700 years and were probably associated with extremely severe droughts (Meggers 1994). Currently, however, economic and demographic growth in the tropics has shortened the frequency of these events to every 5–15 years (Goldammer 1990, Cochrane et al. 1999, Alencar et al. 2006). As the agricultural frontier advances in the Amazon region, the risk of wildfire increases. Pasture and crop areas reduce evapotranspiration and contribute to lower humidity, and the widespread use of land-management practices that involve fire provides ready ignition sources (Nepstad et al. 2001). As a result, forest fires are more common along the forest edge (Laurance et al. 1997, Cochrane 2001, Cochrane and Laurance 2002, Alencar et al. 2004), not only because fires escape from areas of pasture and cropland that are being burned, but also as a result of drier climatic conditions on neighboring deforested areas (Kapos et al. 1993, Gascon et al. 2000). In addition, extensive deforestation may lead to a reduction in rainfall over the Amazon (Sampaio et al. 2007, da Silva et al. 2008), augmenting the risk of loss of a large portion of the Amazon forest to climate change-induced fires as early as 2020 (Golding and Betts 2008). Logging also makes the forest vulnerable to fire by opening the canopy and thus increasing light penetration that lowers humidity and enhances forest flammability (Uhl and Kauffman 1990, Cochrane et al. 1999, Nepstad et al. 2001). In a similar way, fire begets more fire as it kills trees, increasing light penetration and, initially, adding more dry fuel to the forest floor in a vicious positive feedback loop (Nepstad et al. 2001).

In sum, the synergy between deforestation, logging, land management practices associated with fire, and increasingly drier climate may increase fire activity in the Amazon, leading the remaining forests toward a vicious cycle of impoverishment (Nepstad et al. 2001), culminating in a tipping point that may be reached within the next two decades (Golding and Betts 2008, Nepstad et al. 2008).

Despite the striking impacts of fire on tropical forest ecosystems, fire modeling in the tropics is still in its early stages (Cochrane 2003, Balch et al. 2008). One of the major challenges for tropical fire modeling is the absence of data and models on fire fuels, which are crucial to predict the potential for ignition and duration of a fire (Cochrane 2003). Second, the understanding of fire dynamics, and thus fire behavior in different types of fuels and environments, is still limited (Cochrane et al. 1999). Moreover, fire data, including fire duration, burned area, and location, are not available and their acquisition depends on high-resolution remote-sensing imagery combined with fieldwork. In short, wildfire models (e.g., NWGC 2002, Venevsky et al. 2002, CFS 2007) involve multiple components (i.e., ignition and propagation submodels) comprising numerous parameters that still need to be adapted and calibrated to the biophysical characteristics of the diverse Amazon landscapes.

Some studies have attempted to develop models of fire risk for the Amazon. For example, Cardoso et al. (2003) analyzed climatic and biophysical variables to model fire occurrence on a $2.5° \times 2.5°$ cell grid for the dry seasons of 1995 and 1997. Sismanoglu and Setzer (2005) developed a model to calculate the risk of fire at a resolution of 25×25 km for the entire Brazilian territory, taking into account climatic and vegetation variables processed at daily time steps. Nepstad et al. (2004) developed *RisQue*, a model that estimates plant available water (PAW) as an indicator of forest fire risk for the entire Amazon, and Alencar et al. (2004) quantified the relationship between landscape parameters and forest fire occurrence in the eastern Amazon. Most of these studies took advantage of the Fire Monitoring Project, an initiative of the Center for Weather Forecast and Climate Studies (CPTEC) of Brazil's National Institute for Space Research (INPE) that detects burning sites (hot pixels) by using satellite imagery and publishes these data on the Internet (information *available online*).[6] Hot pixels on a satellite image consist of the signal detection of the radiance of fire flames with temperature around 1000 K, whose emission peak is situated in the middle infrared region (e.g., channel 3 in Advanced Very High Resolution Radiometer [AVHRR]: 3.55–3.93 μm). A fire needs to occupy only a small fraction of the total pixel area to saturate the middle infrared channel and thus be detected (Schroeder et al. 2005).

Although hot pixel data do not usually detect understory fires (Nepstad et al. 1999*a*, INPE 2008*a*) and thus do not measure area burned in the forest (INPE 2008*a*), they can be used to map fire occurrence

[6] ⟨www.cptec.inpe.br/queimadas⟩

in close proximity to forest borders that may represent potential ignition sources to forest fires.

Within this context, we developed a model of human-induced fire occurrence for the Amazon region (defined here as the Amazon River Basin, the Brazilian Legal Amazon, and the Guiana shield) that integrates climate and land-use data to simulate monthly occurrences of hot pixel, which represent fire activity within the Amazon forest and along its fringe (a four-km buffer around the forest). We used this model to simulate future fire regimes (i.e., spatial and temporal patterns of fire occurrence) in the Amazon in response to climate change and deforestation in order to estimate potential carbon emissions from forest fires, an important component of REDD (Reducing Emissions from Deforestation and Forest Degradation in Developing Countries), a policy that would be supported through the new climate treaty under negotiation within the United Nations Framework Convention on Climate Change (Nepstad et al. 2009). In addition, the model presented here represents a step towards an integrated model that aims to assess the likelihood of a near-term forest dieback tipping point due to the complex interactions between deforestation, logging, fire, and climate change in the Amazon (Nepstad et al. 2008).

Model Development

The present model estimates the probability of fire occurrence by integrating climatic conditions (as described by vapor pressure deficit [VPD] data) with a series of biophysical and land-use variables, such as elevation, distance to roads and towns, and legal restrictions (i.e., protected vs. non-protected areas). The idea behind this approach is to capture both the anthropogenic land use and weather determinants of fire occurrence. The model follows four steps. First, annual anthropogenic probability of fire, given a set of spatial variables, was obtained by employing Weights of Evidence, a Bayesian method appropriate for modeling spatial data (Bonham-Carter 1994, Soares-Filho et al. 2004). Next, we developed a map of climatic risk by applying logistic regression on monthly VPD data and followed by merging these two probability maps into a single one using a weighted average. The model then used this combined probability map to stochastically simulate the quantity and location of hot pixels at monthly time steps and at a spatial resolution of 2×2 km. Hot pixels that we used consisted of daily fire signal detection by AVHRR aboard the National Oceanic and Atmospheric satellite (NOAA-12) with passages across the equator at 21:00 Coordinated Universal Time. NOAA-12 night satellite hot pixel data from 2003 were used to calibrate the model; the data from this year most closely approximated the mean for the analyzed time period (2002–2005). The model was validated using hot pixel data from 2002, 2004, and 2005.

Finally, we simulated future Amazon fire regimes to the year 2050 under three scenarios: the first consists of the A2 climate scenario of IPCC (Intergovernmental Panel on Climate Change) using simulated data from the Hadley Centre's HadCM3 model (Cox et al. 1999), the second is a business-as-usual (BAU) scenario of deforestation and road expansion from SimAmazonia (Soares-Filho et al. 2006), and the third is the combination of these two scenarios. We then compared the simulated fire regimes under these three scenarios with fire occurrence in the Amazon during the 1999–2005 period. All modeling phases were developed using Dinamica EGO freeware, an innovative environmental modeling platform that holds a complete solution for calibrating, running, and validating space–time models (Soares-Filho et al. 2010*b*). Each of these steps is described in detail in the sections that follow.

Anthropogenic risk of fire

Previous studies have shown that fire occurs more frequently in the Amazon in logged and previously burned forests (Nepstad et al. 1999*b*), and is associated with roads (Cardoso et al. 2003, Alencar et al. 2004) and forest edges (Alencar et al. 2004). In contrast, protected areas and indigenous lands show lower rates of deforestation and fire occurrence than their surrounding areas, which can be considered an inhibitory effect (Nepstad et al. 2006*b*, Soares-Filho et al. 2010*a*). Of these factors, we selected the following variables to compose the anthropogenic risk of fire: (1) distance to deforested or cerrado areas, (2) distance to forest, (3) distance to towns, (4) distance to roads, (5) elevation, and (6) protected areas, including conservation reserves, sustainable use areas, and indigenous lands. All distance variables measure the Euclidian distance between each map cell to the closest map cell of the target feature. These variables were selected because they showed low spatial correlation to each other and strong spatial association with fire occurrence according to the Weights of Evidence analysis. The cartographic data set employed in this work comes from various sources. Elevation is derived from SRTM (Shuttle Radar Topography Mission) maps, towns from IBGE (Instituto Brasileiro de Geografia e Estatística; IBGE 2005), forest and deforested areas from PRODES (Programa de Cálculo do Desflorestamento da Amazônia; INPE 2008*b*), and roads together with protected areas and indigenous lands from data sets compiled by Soares-Filho et al. (2010*a*).

Weights of Evidence is a Bayesian method traditionally used to derive favorability maps for spatial point phenomena (Agterberg and Bonham-Carter 1990, Bonham-Carter 1994, Soares-Filho et al. 2010*a*, *b*). In this study, weights of evidence (W_k^+) are calculated for every k category of each spatial variable under analysis and can be interpreted as the influence of that category on the chances of hot pixel occurrence. Since this method only applies to categorical data, it is necessary to categorize continuous gray-tone variables, such as distance-decay maps; this is done using a method

adapted from Agterberg and Bonham-Carter (1990) in Dinamica EGO (Soares-Filho et al. 2010*b*).

Given a set of spatial variables $\{B_1, B_2, B_3, \ldots, B_k\}$ the probability of a hot pixel is denoted as follows:

$$P(\text{HotPixel} \mid B_1 \cap B_2 \cap B_3 \cap \ldots . B_k)_{(x,y)} = \frac{e^{\sum W_k^+}}{1 + e^{\sum W_k^+}} \quad (1)$$

where $P(\text{HotPixel} \mid B_1 \cap B_2 \cap B_3 \cap \ldots . B_k)_{(x,y)}$ is the probability of occurrence of a hot pixel given a set explanatory variables at a cell location (x, y), and W_k^+ is the weight of evidence coefficient for a category of variable B_k. To derive weight of evidence coefficients for each variable category under consideration, we superimposed the 2003 binary map of hot pixel occurrence within a grid cell of 2×2 km with maps of these variables. In the following sections, $P(\text{HotPixel} \mid B_1 \cap B_2 \cap B_3 \cap \ldots . B_k)_{(x,y)}$ for a year j will be referred to as $\text{Pbiop}_{(x,y),j}$. High positive values for weights of evidence favor the modeled event: the higher the value, the stronger the association. On the other hand, a negative W_k^+ value indicates an inhibitory effect, whereas values close to zero are consistent with no association (Bonham-Carter 1994). The only assumption of this method is that all explanatory variables be independent. In order to test this assumption, we measured the correlation between pairs of variables applying the Joint Information Uncertainty Test (Bonham-Carter 1994). In addition, we evaluated the explanatory power of each variable by comparing the Weights of Evidence Contrast $(W_k^+ - W_k^-)$ for each of the variable categories, so that the most significant variables showed the highest Contrast, and thus, the strongest relation with hot pixel location. The probability map is calculated integrating all the W_k^+ by means of Eq. 1. The anthropogenic-risk probability map is updated on an annual basis employing outputs from SimAmazonia (Soares-Filho et al. 2006), thereby incorporating the effects of new roads and the advance of deforestation.

Climatic risk of fire

Former studies have modeled fire activity using climatic variables such as precipitation, temperature, relative humidity (Cardoso et al. 2003, Sismanoglu and Setzer 2005), and forest flammability using plant available soil water (PAW; Nepstad et al. 2004) and understory vapor pressure deficit (Ray et al. 2005). In this study, we selected vapor pressure deficit (VPD) obtained from meteorological stations (a measure of evaporative demand of the atmosphere that integrates the influence of temperature and relative humidity) as the sole explanatory variable for modeling the influence of climate on hot pixel occurrence for three reasons. First, box plot graphs with monthly values of VPD from hot pixels (Fig. 1) showed a strong positive association between these two variables. Second, as VPD integrates and thus is correlated with other climatic variables commonly applied to fire modeling, such as precipitation history, PAW, and relative humidity, only one of them could be employed in the logistic regression analysis; the best fit was obtained when only VPD was used (Table 1). Third, Ray et al. (2005) have shown that understory VPD, which can be derived from meteorological VPD and forest structural information (e.g., canopy height, leaf area index), is a strong predictor of forest flammability. Monthly VPD means were obtained from a subset of 266 meteorological stations distributed throughout the Amazon and interpolated to generate monthly maps from 1995 to 2005 at a grid resolution of 8×8 km (Hirsch et al. 2004).

Due to the fact that climate seasonality differs in the northern and southern hemispheres, we had to develop a general model that could describe the climatic risk for fire on a monthly basis throughout the year and across the entire Amazon. Therefore, we tested different approaches to derive a single relationship that could be applied to all different regions and seasons. The best approach consisted of adjusting a separate logistic regression for each month, in which the response variable is the binary hot pixel occurrence within 2×2 km grid cell and the explanatory variable is the monthly mean VPD, and then estimating the average equation that could be used in all months, as follows:

$$\text{Pcl}_{(x,y),i,j} = \frac{e^{\beta_{0i} + \beta_{1i}\text{VPD}_{(x,y),i,j}}}{1 + e^{\beta_{0i} + \beta_{1i}\text{VPD}_{(x,y),i,j}}} \quad (2)$$

where $\text{Pcl}_{(x,y),i,j}$ represents the probability of a hot pixel given VPD in cell (x,y) in month i and year j, and β_{0i} and β_{1i} are the parameters of the logistic regression for month i. By replacing the β_{0i} and β_{1i} values with the 2003 mean values, we obtained the formula expressed in Eq. 3, which is the general equation for calculating the monthly climatic risk for the time series under analysis:

$$\text{Pcl}_{(x,y),i,j} = \frac{e^{-5.0820 + 4.1005\text{VPD}_{(x,y),i,j}}}{1 + e^{-5.0820 + 4.1005\text{VPD}_{(x,y),i,j}}}. \quad (3)$$

Integrating anthropogenic and climatic risks

Forest fire risk is determined by a combination of anthropogenic factors and favorable weather conditions. Hence, our approach consisted of merging both anthropogenic and climatic risk maps into one. After testing several approaches to generate a probability of fire that accounted for both biophysical and climatic factors (e.g., combining the two probability maps using the Weights of Evidence method or through geometric averaging), we chose to weight average the two maps using different weight values according to periods of the year (Eq. 4), given that this approach yielded the highest Relative Operating Characteristic (ROC) indices (ROC is a method for evaluating favorability/probability maps vs. observed data [Pontius and Schneider 2001]):

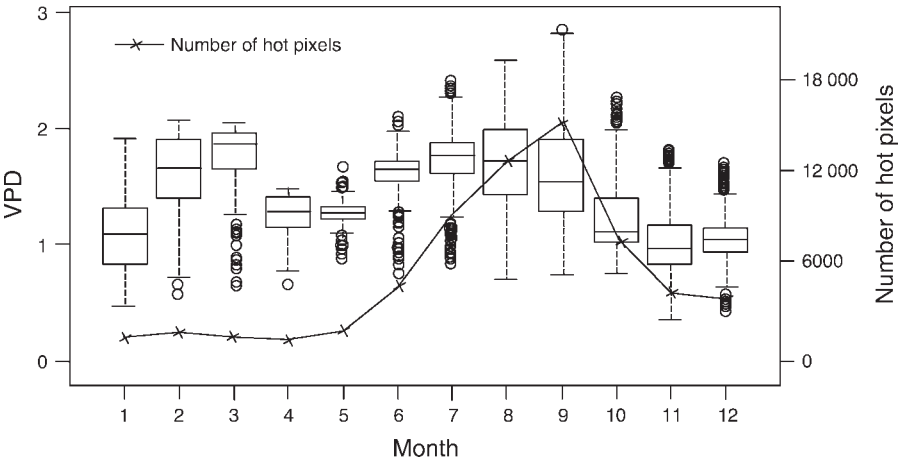

FIG. 1. Box plots of vapor pressure deficit (VPD) and number of hot pixels for 2003. For each month, boxplot graphs show a summary of VPD statistics: median (center line), first quartile (lower box bound), third quartile (upper box bound), outliers (circles), sample minimum excluding outliers (horizontal lower bar), and sample maximum excluding outliers (horizontal upper bar). There is a positive association between VPD and number of hot pixels. In the beginning of the year, the number of hot pixels is low and so are the lower boundaries of the VPD box plots. From May onward, hot pixel number increases until August and September, and then declines again at the onset of the rainy season, showing the same seasonal pattern as VPD.

$$P_{(x,y),i,j} = \alpha_i \mathrm{Pbiop}_{(x,y),j} + (1 - \alpha_i)\mathrm{Pcl}_{(x,y),i,j} \quad (4)$$

where $P_{(x,y),i,j}$ is the combined probability of hot pixel occurrence for a cell (x, y) in month i of year j. $\mathrm{Pbiop}_{(x,y),i,j}$ is the probability of fire given a set biophysical factors in year j, and $\mathrm{Pcl}_{(x,y),i,j}$ represents the probability of fire given climatic conditions for month i of year j.

We chose α values in order to simultaneously maximize ROC statistics of $P_{(x,y),i,j}$ for all months of 2003. As a result, this parameter assumed a value of 0.2 from January to April and 0.4 for the other months. In essence, this latter value relates loosely to the burning season associated with deforestation in the southern Amazon, which extends into December. The values we found for α suggest that fire risk is more directly impacted by climatic than anthropogenic factors, possibly because favorable weather conditions are a precondition for human-induced fires.

Simulation of fire occurrence

Our model stochastically simulates the occurrence of hot pixels at monthly time steps using the combined fire risk probability map and taking into account the spatial and temporal dependence between hot pixels. The spatial dependence between fire events has already been considered for predicting fire occurrences (Sismanoglu and Setzer 2005). In this work, we tested the spatial dependence between hot pixels for each month of 2003 by employing the Moran Autocorrelation Index, which was normalized to a $\{-1, 1\}$ interval to facilitate interpretation (Bailey and Gatrell 1995). The Moran Autocorrelation Index indicates the extent to which the occurrence of a hot pixel influences the occurrence of

TABLE 1. Percentage agreement between observed and predicted hot pixels per month using the climatic probability risk equation (Eq. 3).

Month	Hot pixels predicted : observed (%)				Total correct classification (%)
	1:1	1:0	0:1	0:0	
Jan	16	7	24	53	69
Feb	38	6	3	54	91
Mar	38	5	2	56	94
Apr	21	8	19	52	74
May	34	9	6	51	85
Jun	39	15	1	46	85
Jul	65	12	1	21	87
Aug	61	13	6	20	81
Sep	57	15	9	18	76
Oct	14	19	26	41	55
Nov	16	51	7	27	42
Dec	8	5	43	45	53

Note: The "total correct classification" column corresponds to the sum of the second and fifth columns. The values 0 and 1 are binary factors indicating occurrence (1) or absence (0) of fire, for both simulated and observed hot pixels.

TABLE 2. Adjusted Moran's autocorrelation index by month and respective *P* values for 2003 monthly hot pixel data.

Month	Moran's index value	*P*
Jan	0.139	0.003
Feb	0.305	0.002
Mar	0.221	<0.001
Apr	0.215	0.002
May	0.294	<0.001
Jun	0.386	<0.001
Jul	0.392	<0.001
Aug	0.316	<0.001
Sep	0.283	<0.001
Oct	0.245	0.002
Nov	0.179	0.002
Dec	0.229	0.003

another one in neighboring cells. This test was significant ($P < 0.05$), demonstrating a positive dependence between nearby hot pixels, in particular for the dry-season months (Table 2).

The next step consisted of identifying the probability density function of the hot pixel occurrences, a standard procedure for developing stochastic simulations. The density function of the monthly fire risk maps for 2003 hot pixels showed that the probability functions from January to September matched a Beta (0.985;0.1) distribution truncated at 0.5, while those from October to December approximated a Weibull (13;0.6) distribution. These distributions were employed to draw random numbers for the cell selecting mechanism so that for each cell, a hot pixel would occur if

$$(\rho_{(x,y),i,j} - \gamma_i) < P_{(x,y),i,j} < (\rho_{(x,y),i,j} + \gamma_i) \quad (5)$$

where $P_{(x,y),i,j}$ is the probability of hot pixel occurrence; $\rho_{(x,y),i,j}$ corresponds to a random number drawn from the probability density function according to month i of year j for the (x,y) cell, and γ_i is a constant (Table 3) used to control the number of simulated hot pixels by increasing the acceptance interval.

In order to incorporate the spatial and temporal dependences between hot pixels, we divided the cell-selecting process into 10 loops, each one analyzing only 10% of the total number of cells, so that after the 10th iteration the entire map has been completely analyzed. After each loop, the spatial dependence is incorporated into the model, multiplying the probability of neighboring cells (considering a Moore neighborhood of eight adjacent cells) of simulated hot pixels by 1 plus the Moran Index of the corresponding month (Table 2) and limiting the maximum probability value to 0.9999 to avoid probabilities greater than or equal to 1. Because the number of hot pixels depends on the map resolution, the last procedure within the loop consists of sampling only a percentage of selected cells to become simulated hot pixels by applying a pruning factor according to Table 4. Both γ and pruning factor values were established by interactively maximizing the match between the simulated number of hot pixels with observed ones.

TABLE 3. The γ values obtained in the simulation for two time periods.

Months (*i*)	γ_i
Jan–Apr and Oct–Dec	0.05
May–Sep	0.09

Note: In the simulation, γ values are used to customize the acceptance interval of hot pixel occurring to the climatic characteristics of each month, controlling as a result the number of simulated hot pixels according to seasonal variability.

TABLE 4. Pruning factors control the number of fire occurrence by keeping only a percentage of selected cells as simulated hot pixels.

Months (*i*)	Pruning factor *i*
Jan–May	0.995
Jun, July, and Oct–Dec	0.999
Aug and Sep	0.997

Model validation

We validated the model by comparing its predictions to the observed data for 2002, 2004, and 2005 on a monthly basis using three fitness measures. One is the Relative Operating Characteristics (Pontius and Schneider 2001). ROC statistics measure the level of agreement between a probability or favorability map and a map with the observed events (in this case, the map of actual hot pixels). A value of 1.0 indicates a perfect match, whereas values close to 0.5 can be expected due to chance.

The second method applies a fuzzy map comparison between the monthly simulated and the observed hot pixels (Almeida et al. 2008, Soares-Filho et al. 2010*b*). This method compares the number of cells of a certain class in a simulated map with the number of these cells in a reference map that fall within a central cell neighborhood, as defined by a window size. By using a constant decay function, if a matching cell is found within the window, fit is assigned to 1, and otherwise takes on a value of 0. Windows with increasing sizes convolute over the map and a mean is computed for each window size. This method employs a reciprocal approach, comparing the match between map 1 and map 2, and vice versa, ultimately choosing the minimum mean in order to penalize random maps, which tend to overestimate the fit. In this manner, this method accounts for both omission and commission errors. Our comparison employed increasing window sizes from 1 to 11 cells, which in terms of spatial resolution represent a range from 2×2 km to 22×22 km. Finally, the third method compares the total number of simulated hot pixel cells to observed hot pixel cells on a monthly basis using time series graphs.

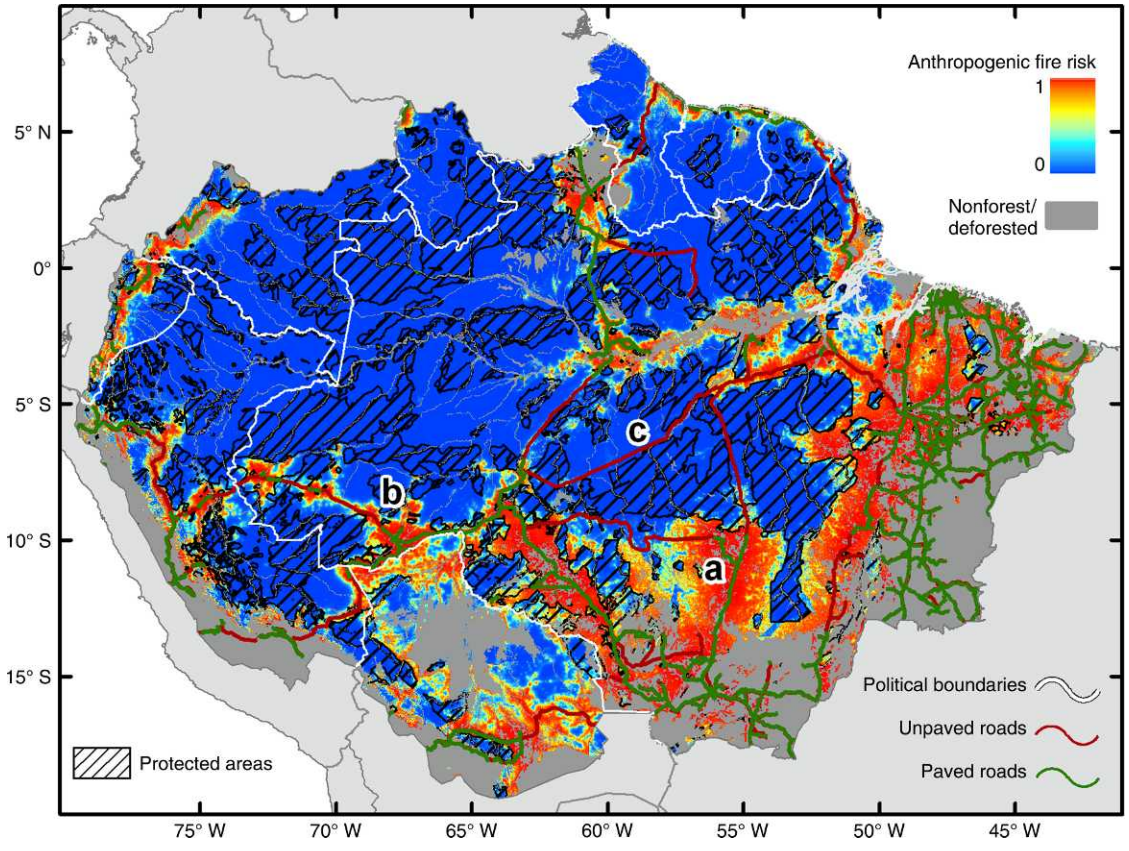

FIG. 2. Risk of fire given biophysical and anthropogenic variables for 2004. For anthropogenic risk, the values 0 and 1 indicate, respectively, minimum and maximum risks. The highways are represented by: (a) BR-163 (Cuiabá-Santarém), (b) BR-319 in Acre, and (c) BR-230 (Transamazon Highway).

Projecting future fire regimes

Climate model experiments predict that large portions of the Amazon forest may be replaced by savanna-like vegetation as a consequence of climate change (Cox et al. 2000, 2004, Botta and Foley 2002, Oyama and Nobre 2003, Collins 2005, Li et al. 2006, Salazar et al. 2007). However, none of these experiments include the effects of fires on the Amazon forest. In order to fill this gap, we applied the Hadley Centre HadCM3 projections for the IPCC's A2 scenario to evaluate the role of climate change in the Amazon fire regime. We chose this model because it successfully replicates the effects of El-Niño droughts on the climate in the Amazon (Collins 2005, Cox et al. 2008), and thus, it is widely used to simulate climate change over the Amazon (e.g., Cox et al. 2000, 2004). Among the IPCC scenarios that do not consider climate change mitigation efforts, the A2 scenario presents the highest CO_2 emission rates due to a steady increase in global population, economic growth, and no advances in renewable energy. By 2100, under this scenario, temperatures are expected to rise between 2°C and 5.4°C (IPCC 2007). The A2 scenario is currently considered very plausible, given the increase in anthropogenic carbon emissions due to global economic growth (van der Werf et al. 2009).

Projected VPD under the A2 scenario, HadCM3 model, was obtained through a combination of temperature and relative humidity data, which were downloaded from the WCRP (World Climate Research Programme), CMIP3 (Coupled Model Intercomparison Project), Multi-Model Data Base (ESG 2009). In order to correct the mismatch between climate projections and observed climate in the Amazon, we used the same methodology of Malhi et al. (2009); i.e., we calculated a ratio between HadCM3 model's VPD monthly data from 2006 to 2050 and the ones from 2000 to 2005, and then we applied this ratio to our VPD monthly 2000–2005 grid data to represent VPD time series from 2006 to 2050.

In addition, we used the results of the SimAmazonia model under the BAU scenario to add the effects of deforestation and road expansion on the Amazon fire regime. The BAU scenario assumes that deforestation rates will increase in the future due to the combination of paving a series of highways across the Amazon and lax environmental law enforcement (Soares-Filho et al. 2006).

With the Hadley Centre model and SimAmazonia data, we established three scenarios: (1) climate change,

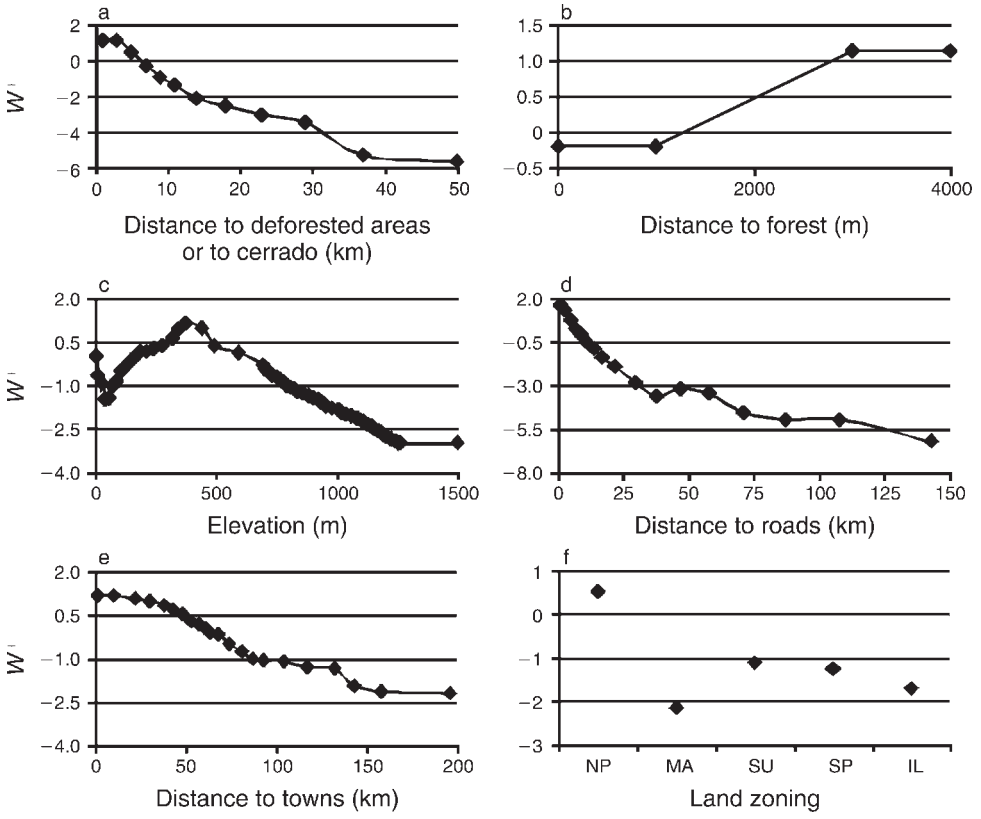

FIG. 3. Weights of Evidence (W^+) graphs for the following variables: (a) distance to deforested areas and Cerrado, (b) distance to forest, (c) elevation, (d) distance to roads, (e) distance to towns, and (f) land zoning (NP, non-protected; MA, military area; SU, sustainable use; SP, strict protection; and IL, indigenous land). Positive values indicate association with fire events, and negative values repulsion.

deforestation, and new paved roads; (2) only climate change; and (3) only deforestation and new paved roads, and then compared the fire regimes under each modeled scenario with the current climate and land-use conditions by computing the mean annual number of hot pixels from 2010 to 2050 in quadrats of 50×50 km.

Estimating committed carbon emissions from deforestation and forest fire

We calculated committed carbon emissions (Fearnside 1997) from deforestation by superimposing simulated deforested cells on a map of forest biomass (Saatchi et al. 2007), and assuming that carbon content is 50% of wood biomass (Houghton et al. 2001) and that 85% of the carbon contained in trees is released to the atmosphere through deforestation (Houghton et al. 2000). However, hot pixel distribution does not provide a direct estimate of burned forest area that can be used to calculate emissions from forest fires. In order to do this, we compared the number of hot pixels within the Amazon forest with the extent of forest areas that actually burned in the Brazilian Amazon in 2005 (Lima et al. 2009) to derive a ratio between hot pixel density and burned forest area. Then, we calculated the total number of hot pixels in each simulation year that fell within the forest and applied the resulting hot pixel/burned forest ratio to infer the total burned forest area per forest carbon biomass class of the map provided by Saatchi et al. (2007). Carbon emissions from burned pastures and other land uses were not considered. Finally, we estimated committed carbon emission from forest fires using Eq. 6, according to Alencar et al. (2006):

$$K = 0.5\lambda \sum_i A_i B_i \tag{6}$$

where K is the total committed carbon emissions from forest fires (in grams), assuming that half of tree biomass killed by fire will be ultimately released to the atmosphere through decomposition (Fearnside 1997), λ is tree mortality (percentage of biomass killed by fire), A_i is the burned forest area (hectares) per biomass class, and B_i is the biomass density per class i (grams per hectare). Tree mortality rate may vary from 10% to 50% depending on fire intensity and the state of the forest (Alencar et al. 2006). For tree mortality (λ), we assumed conservative values of 10%–20% and added uncertainty bounds of 20% to take into account errors in biomass measurement for both deforestation and fire emission estimates (Chave et al. 2004). Thus, while our calcula-

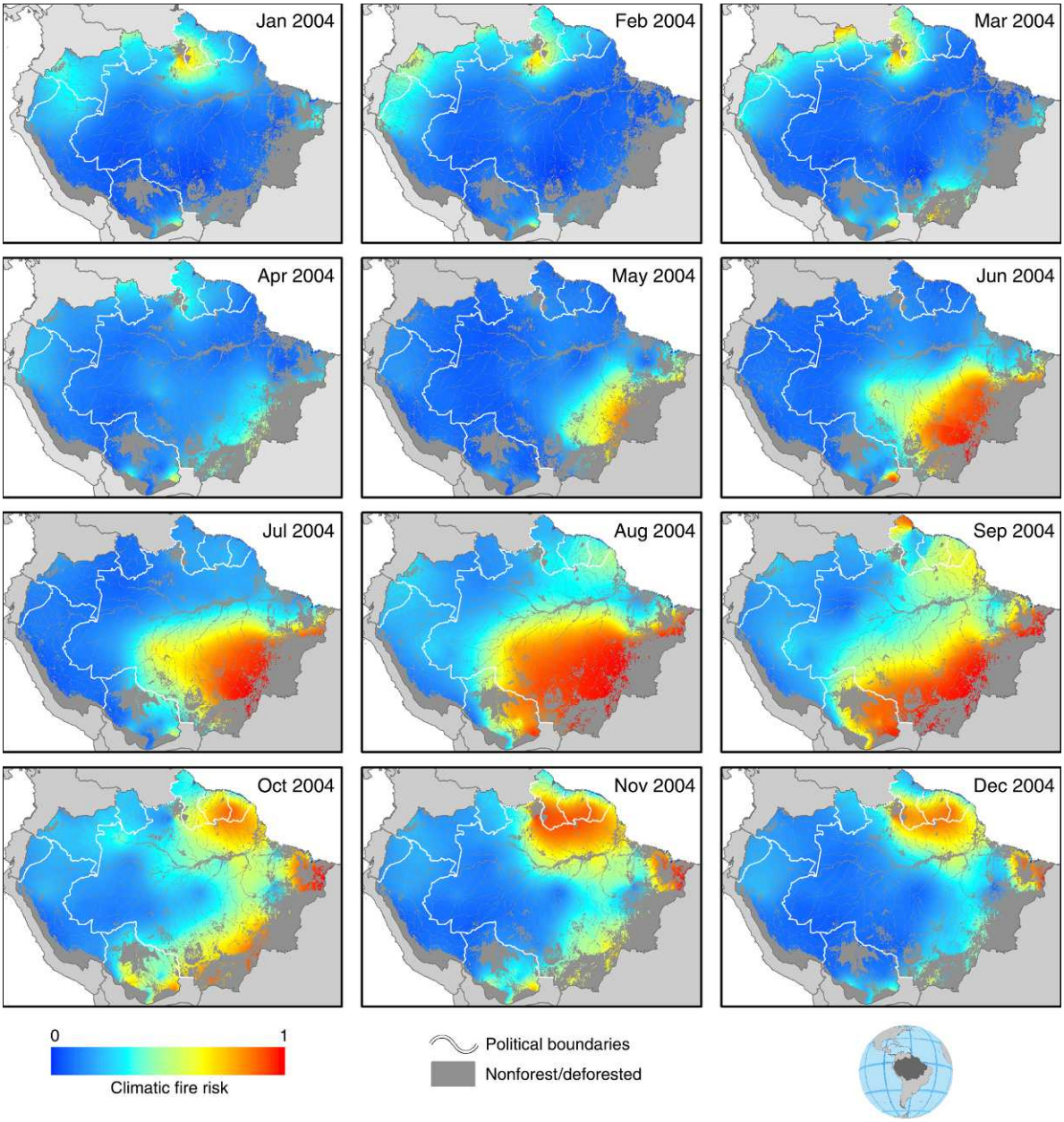

FIG. 4. Monthly climatic fire risk for 2004. For climatic fire risk, the values 0 and 1 indicate, respectively, minimum and maximum risks.

tions may underestimate carbon emissions from forest fires, they do not account for forest regrowth that occurs following a fire (Alencar et al. 2006).

RESULTS

Fig. 2 shows fire risk for 2004 given the selected set of biophysical and land-use variables. The probability map indicates a strong inhibitory effect of protected areas and indigenous lands on hot pixel distribution, as already pointed out by Nepstad et al. (2006*a*). Conversely, hot pixels closely follow deforestation and major roads, such as the BR-163 (Cuiabá-Santarém), the BR-319 (Manaus-Porto Velho), BR-364 in Acre, and BR-230 (Transamazon Highway) (Fig. 2), demonstrating the strong association of fire with forest clearing and pasture maintenance practices.

Fig. 3 depicts the spatial function for each of these factors. Positive weights of evidence for forest near deforested areas highlight the major effect of forest fragmentation in facilitating forest fire (Alencar et al. 2004). In accordance with previous studies (Laurance et al. 2001, Cardoso et al. 2003), proximity to roads is

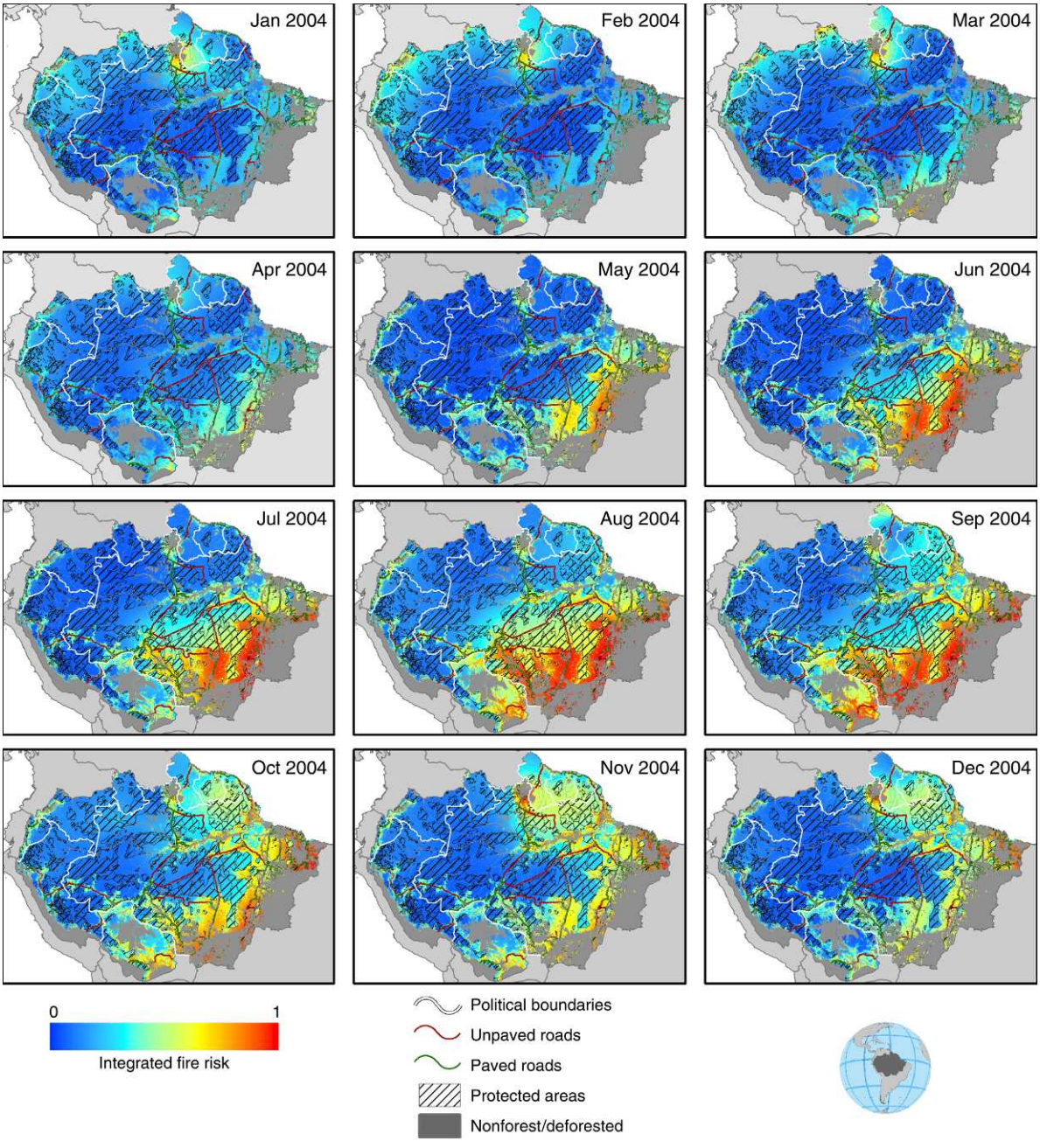

FIG. 5. Monthly integrated fire risk for 2004. For integrated fire risk, the values 0 and 1 indicate, respectively, minimum and maximum risks.

another high risk factor; forests located within an eight-km border of roads are highly vulnerable to fire. Distance to town centers showed a similar effect, although with lower absolute values. There is a negative association between hot pixels and elevation up to 70 m, probably related to flood plains and wetlands. From 70 m to 690 m, the chance of fire tends to increase, as land becomes terra firme (non-flooded land), then from 700 m upwards, this tendency reverses again. Notably, the protected area and indigenous land network greatly controls the spatial distribution of hot pixels, showing negative weights of evidence; the weights of evidence exhibit the lowest values for indigenous lands and military areas.

In addition, seasonal climatic patterns across the Amazon control the risk for fire (Fig. 4). In the beginning of the year, the dry season north of the equator increases fire risk in that region. As the year unfolds, the high-probability zone moves southward and expands until it reaches a maximum in August. In

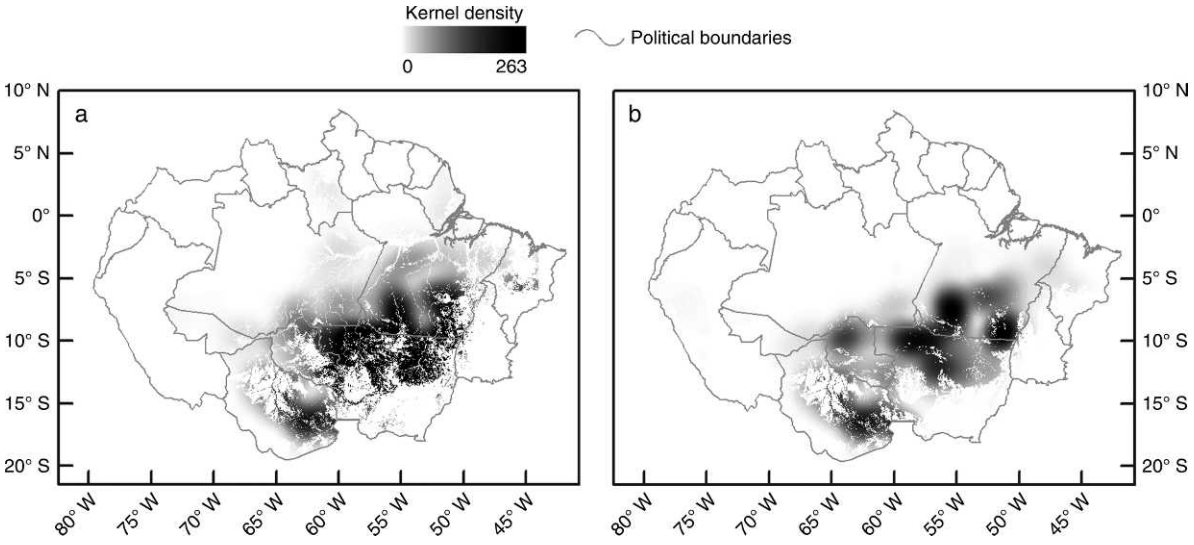

FIG. 6. Kernel density for (a) observed hot pixels and (b) simulated hot pixels for August 2004. Observed hot pixels appear more clustered than the simulated ones.

October, at the onset of the rainy season in the southern hemisphere, this zone moves toward the northeast, confining itself again to the north of the Amazon by the end of the calendar year. This pattern is repeated in annual cycles with the high-risk zone becoming larger and more persistent in years of severe drought. A cross-tabulation of observed vs. predicted hot pixels from the monthly logistic regressions (Table 1) show that VPD can better predict fire risk during the dry-season months and in February and March, which showed especially high accuracy scores.

The combined map of fire risk follows the same temporal pattern as the climatic risk map with greater specificity added by anthropogenic risk factors, such as the presence of roads or protected areas (Fig. 5). Presence of roads enhances the risk of fire only if weather conditions are favorable. On the other hand, risk of fire is always higher near deforested areas and the inhibitory effect of protected areas becomes more conspicuous as dry weather conditions persist. Assessment of the monthly fire probability maps yielded ROC fitness values >85% for all months from 2002 to 2005, thus demonstrating their likelihood in revealing the high-risk zones for fire. This prediction is more accurate from February to June, in contrast to the period from October to December.

With respect to the simulation of hot pixels, although spatial dependence was incorporated into the model, the observed hot pixels are still more clustered than the simulated ones in all months (Fig. 6). Nevertheless, the agreement between the two maps, as measured by the fuzzy map comparison achieved a match of 60%–70% in September within a window size of 11 by 11 cells (resolution of 22×22 km). Again, the driest months of the Southern hemisphere (June to September), and February and March, showed the highest degree of agreement between observed and simulated hot pixels, whereas the model performed more poorly from October to January.

In terms of quantity, the number of simulated hot pixels follows the same monthly temporal distribution as the observed ones (Fig. 7), showing a maximum annual deviation of 15%. As 2003 data were used to calibrate the model, this year presented the lowest level of deviance between observed and simulated hot pixels. In general, the model tends to overestimate the quantity of hot pixel cells in August, September, and October, whereas it underestimates the quantity in the other months. In this regard, our model could be fine-tuned by adopting different parameter coefficients for each month. However, this procedure would make the model less generalized. Moreover, the model's ability to simulate the abnormally high density of hot pixels in the southwestern Amazon in 2005, in close association with the widespread fires of that particular year, lends support to its applicability for fire prediction (Fig. 8). The graph of Fig. 8 shows that, from 2002 to 2004, the number of simulated hot pixels closely matched observed ones, with peaks occurring in September. The same pattern was obtained for 2005, with high frequency peaks occurring in August and September.

The simulations of future fire regimes to 2050 revealed two main findings: Climate change alone may spread fire activity into the northwestern Amazon, reaching the highly moist forests that are currently resistant to fire (Fig. 9), and the 120% simulated increase in the number of hot pixels outside protected areas under the combined scenario of climate change and deforestation suggests that fire occurrence in those areas may double by midcentury (Fig. 10).

Fig. 9d indicates that forests in the northwestern Amazon may become susceptible to fire only as a result

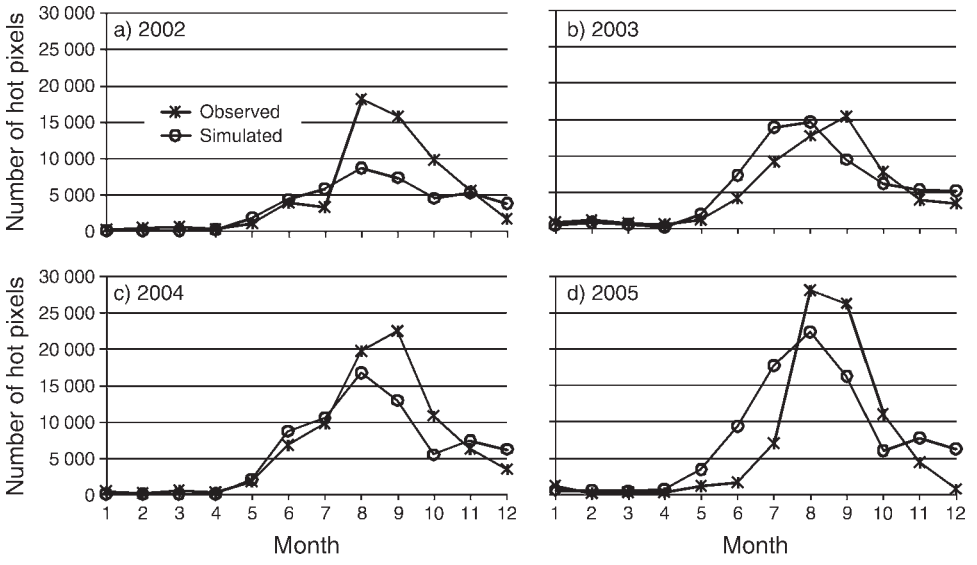

FIG. 7. Time series graphs of observed and simulated hot pixels for (a) 2002, (b) 2003, (c) 2004, and (d) 2005.

of climate change. In turn, Fig. 9b and c show that, although the highest percentage of fires remains along the arc of deforestation, there will be a substantial increase in number of fires along the highways planned for paving (especially along the Transamazon Highway and the BR-319) and in the agricultural zones of Brazil and Bolivia, where forest fires may become even more widespread.

Regarding predicted change in annual fire occurrence between 2010 and 2050 (Fig. 10), 19% increase in number of hot pixels outside protected areas can be attributed to deforestation and road expansion, while climate alone accounts for a 12% increase (Table 5). However, the synergy between climate change and deforestation may increase the number of hot pixels outside protected areas by 49% during this period. Additionally, a scenario of A2 global warming and uncurbed deforestation may increase by half fire occurrence in the Amazon by 2050 (Table 5), and in years of extreme drought, fire occurrence in the Amazon may double outside protected areas (Fig. 10). Under this combined scenario, committed emissions from forest fire and deforestation may amount to 21 ± 4 Pg of carbon by 2050.

DISCUSSION

In this study, we developed a probabilistic approach for modeling fire occurrence in the Amazon. It is important to note that the majority of simulated hot pixels do not represent understory fires (Nepstad et al. 1999*a*), but slash-and-burn, forest clearing, or pasture maintenance practices. These activities, however, can spark major wildfires that expand into the forest for several kilometers, such as the fires that burned in the state of Acre in 2005 (Aragão et al. 2007). As such, we anticipate that the model presented here will serve as an essential component for modeling ignition sources in a more complex fire ignition/propagation model. More detailed land-use maps, which include not only forest and deforested classes, but also differentiate between ranching and crop farming and between large properties and small landholders, will increase the accuracy of fire prediction, given that fire is highly associated with land management practices within a specific set of land-use activities (Alencar et al. 2006). For example, wildfires can diminish in regions with a greater concentration of agro-industrial annual crop production (D. Nepstad, *unpublished data*). In addition, increasing the density of the regional meteorological station grid will allow for improved model performance at finer spatial resolutions. However, at this stage, there is no need to increase the model resolution, since validation showed that model only attains a spatial fitness of 60% to 70% as

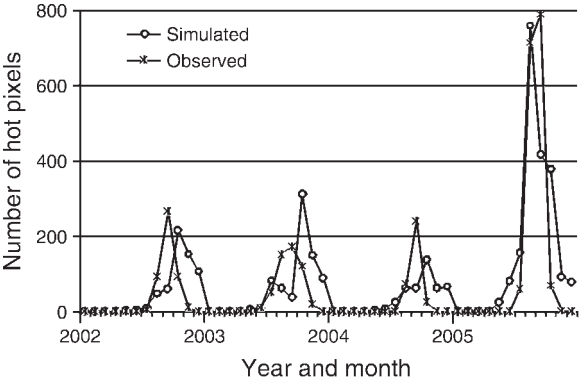

FIG. 8. Time series graphs of observed and simulated hot pixels for the state of Acre, Brazil. These results demonstrated the model ability in simulating the correct number of hot pixels under abnormal climate conditions.

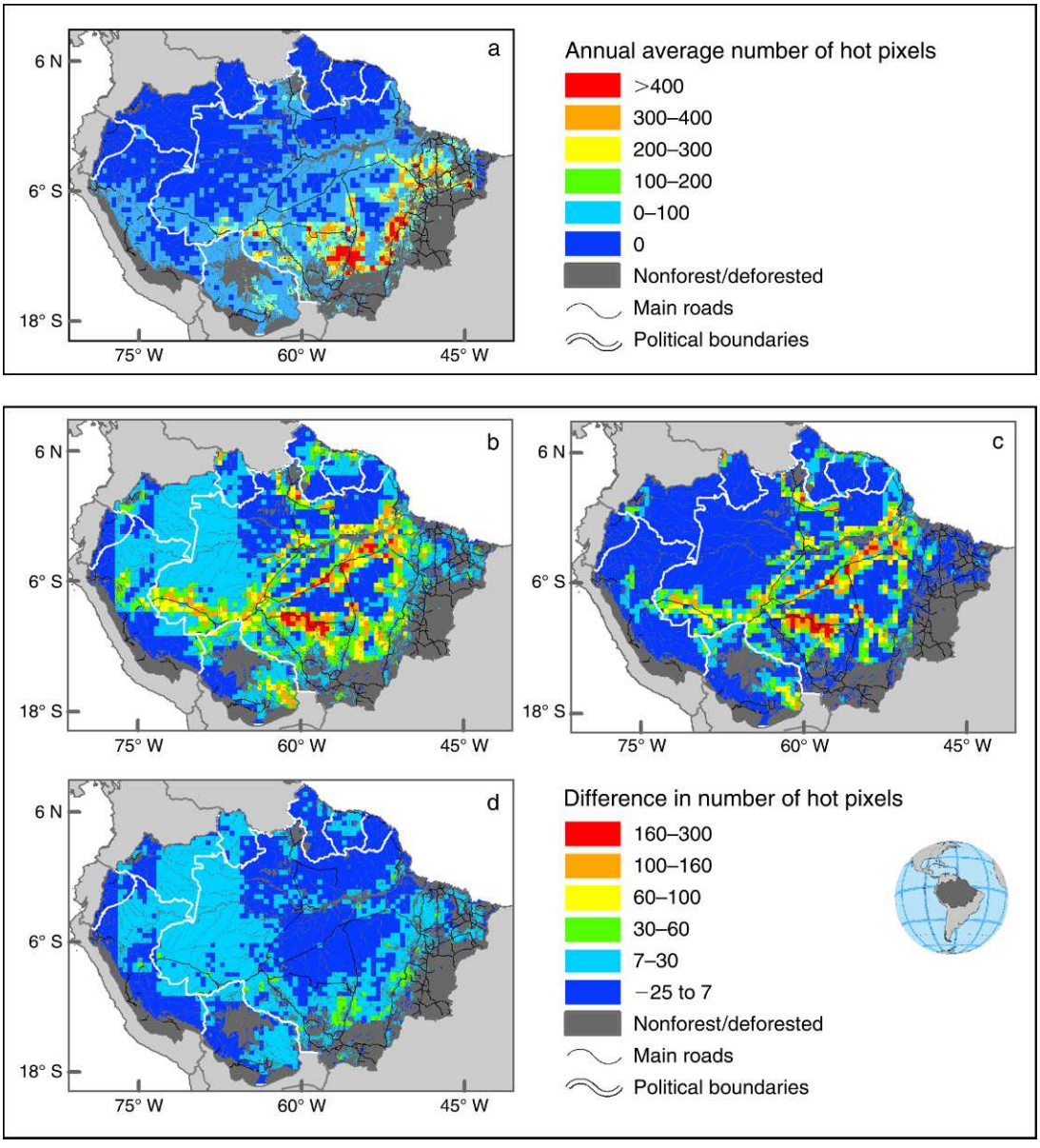

FIG. 9. (a) Average number of hot pixels per 50 × 50 km quadrat under current climate and land-use conditions and difference in number of hot pixels by 2050 in relation to the current conditions for the scenarios: (b) IPCC's A2 climate scenario and business-as-usual (BAU) deforestation, (c) only BAU deforestation, and (d) only A2 climate scenario.

spatial resolution decreases beyond 20 × 20 km. Nevertheless, with respect to providing support to regional fire-prevention programs, this spatial radius is readily accessible by local fire brigades (e.g., Aliança da Terra; information *available online*).[7] Moreover, due to the way that cells are stochastically selected by the model, the number of simulated hot pixel cells becomes highly dependent on the map cell resolution. As we double model resolution, we need to increase the sampling factor used to prune hot pixel cells in the simulation process by a power of 2.

The present model represents a step toward a thorough fire ignition-propagation model. In contrast to the coarse-resolution approach of land surface–climate models (e.g., Gordon et al. 2000, Kucharik et al. 2000, Delire et al. 2004), this type of model needs a finer scale (<500 m or less spatial resolution) to be able to incorporate terrain features, such as land-use barriers, slopes, and river channels, as well as local prevailing wind directions. In addition, a fire propagation model must include fuel load dynamics in order to simulate fire

[7] ⟨www.aliancadaterra.org.br⟩

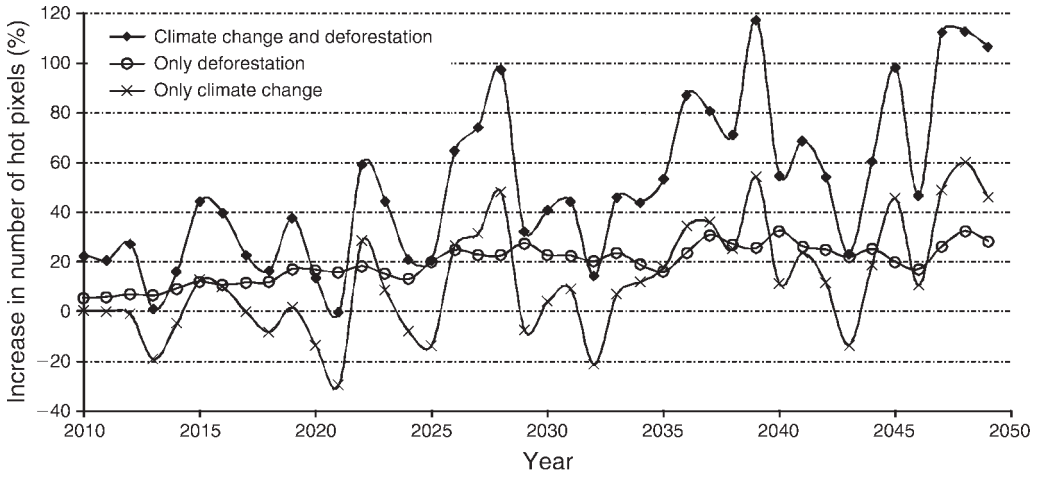

FIG. 10. Percentage increase in number of hot pixels outside protected areas in relation to current climate and land cover conditions.

spread and duration in different environments and weather conditions, as well as to incorporate feedbacks between forest disturbance events, such as logging and recurrent fires. In this respect, field fire experiments conducted in the Xingu headwaters in the Southern Amazon have demonstrated that leaf litter consists of the main fuel load for understory fires; after a fire, the chances of additional fires in the same location in the subsequent two years increase; however, in the third year, fire spread is constrained by insufficient fuel loads (Balch et al. 2008).

In general, fine-scale versions of fire models adopt a process-based approach (e.g., Rothermel 1972, Albini 1996, Butler et al. 2004, Cruz et al. 2005, 2006), which requires the calibration of numerous parameters that describe the physics of fire, such as wind profile, energy transfer, fuel conditions, topography, and flame depth and height. However, the design of such a model that accounts for the diversity of Amazon landscapes could become an insurmountable task due to the lack of calibrated equations and data for modeling the physics of fire in tropical environments. Instead, a more

TABLE 5. Comparison of the main results from modeled scenarios.

Output	NoDefor_NoCC	Defor_NoCC	NoDefor_CC	Defor_CC
Annual mean values for 2010–2050 period				
Number of hot pixel cells within the forest	148 238	118 016	149 936	135 106
Estimated burned forest area (km^2)	22 236	17 702	22 490	20 266
Predicted deforestation (km^2)†	...	43 564	...	43 564
Carbon emissions from fire (Pg)	0.031 ± 0.012	0.023 ± 0.009	0.034 ± 0.014	0.026 ± 0.010
Accumulated values for 2010–2050 period				
Increase in hot pixel cells outside PAs from constant scenario (%)	...	19	12	49
Carbon emissions from fire (Pg)	1.2 ± 0.5	0.9 ± 0.4	1.4 ± 0.5	1.0 ± 0.4
Carbon emissions from deforestation (Pg)	...	19.9 ± 4.0	...	19.9 ± 4.0
Total emissions	1.2 ± 0.5	20.8 ± 4.3	1.4 ± 0.5	20.9 ± 4.4
Annual mean values for 2040–2050 period				
Increase in hot pixel cells from current conditions (%)‡	...	13	25	49

Notes: Abbreviations are: NoDefor_NoCC, no deforestation and no climate change (current climate and land-use conditions); Defor_CC, deforestation, new paved roads, and climate change; NoDefor_CC, only climate change; Defor_NoCC, only deforestation and new paved roads; PAs, protected areas. Note that absolute values of hot pixels, burned forest, and fire emissions are reduced in scenarios in which deforestation takes place due to a constant decrease in size of the remaining forest. Ellipses indicate that the statistic is not applicable to the scenario result. Uncertainty bounds consist of the difference between the maximum emission value minus the minimum from mortality rates that we used, multiplied by 1.2 to account for biomass estimate errors. Thus, the error is plus or minus half of this interval. See *Model development* for a detailed explanation of the error estimate.

† Soares-Filho et al. (2006).

‡ Current climate and land-use conditions.

straightforward approach consists of adopting a probabilistic framework similar to the one presented here to model the relationship between the state of the forest and fire behavior. Because this approach is data driven, it can easily incorporate new data from field experiments, as well as take advantage of heuristic calibration methods, such as genetic algorithms (Koza 1992) and neural networks (Haykin 1999), which are becoming increasingly user-friendly (e.g., Soares-Filho et al. 2010*b*). Moreover, fine-scale, process-based fire models when coupled to carbon fluxes models, such as CARLUC (Hirsch et al. 2004), could improve estimates of carbon emissions from forest fires, whose uncertainty bounds still remain large. These models incorporate the effects of climate seasonality on the vegetation phenology (Xiao et al. 2005, 2006, Huete et al. 2006) and thereby simulate post-fire regeneration, fuel load build-up, and thus forest flammability, while keeping track of carbon fluxes between forest pools and from the forest to the atmosphere due to a fire event.

Therefore, our approach to modeling fire occurrence was to develop a model that could perform well for the entire Amazon in response to land-use and climate seasonality, as well as interannual variability. In comparison to previous models of fire for the Amazon, our model is the first to be thoroughly validated and to include the inhibitory effect of protected areas. We expect that forthcoming availability of monthly basin-wide maps of forest fire scars will allow us to refine the current version of the model.

Conclusion

Climate change combined with continued deforestation and the paving of roads may greatly degrade the Amazon forest, not only by increasing fire occurrence, but also by contributing to the spread of fire into the highly moist forests of northwestern Amazon, which are currently resistant to fire. In particular, forest fires may increase substantially across southern and southwestern Amazon, especially along the highways slated for paving and in the agricultural zones of Brazil and Bolivia. Committed emissions from Amazon forest fires currently average 0.03 ± 0.01 Pg of carbon per year. Climate change alone could increase this range of emissions by 25% after 2040, thus having strong implications for the carbon balance of the Amazon forest even if deforestation ends (Nepstad et al. 2009). However, the synergy between climate change and deforestation may further aggravate the impact of fire on the Amazon forest ecosystems, while exacerbating global warming. Under the A2 climate scenario and uncurbed deforestation, a total of 21 ± 4 of the 86 ± 17 Pg of carbon contained in the Amazon forests (Saatchi et al. 2007) would be released to atmosphere by 2050. Even so, our predictions may be conservative since our model does not incorporate feedbacks between vegetation and climate (Botta and Foley 2002, Oyama and Nobre 2003, Li et al. 2006, Salazar et al. 2007), nor does it account for an increase in frequency of drought years due to El-Niño events (Cândido et al. 2007).

In this respect, climate model experiments predict a substitution of a large portion of the Amazon forest for savanna-like ecosystems by the end of the 21st century in response to global warming (Cox et al. 2000, 2004, Botta and Foley 2002, Oyama and Nobre 2003). In addition, expanding global demands for agricultural products and biofuels (Nepstad et al. 2006*a*, 2008) together with infrastructure investments in the Amazon (Carvalho et al. 2001) may push the agricultural frontier and the timber industry faster and further into the core of the Amazon region (Soares-Filho et al. 2006, Nepstad et al. 2008, Merry et al. 2009). As a result, positive feedbacks in the forest fire regime due to deforestation, logging and climate change may drive a rapid process of forest degradation that could lead the Amazon ecosystem into a cycle of impoverishment (Nepstad et al. 2008). There is still a need to develop simulations that include these synergistic effects of land-use change and fire on the climate–vegetation balance. Therefore, the present model represents a step toward an integrated model that aims to assess the likelihood of a near-term forest dieback tipping point due to the complex interactions between deforestation, logging, fire, and climate change in the Amazon.

Here we showed that continued BAU deforestation may increase fire occurrence by 19% outside protected areas over the next four decades, while climate change alone may account for a 12% increase. In turn, the combination of climate change and deforestation may boost fire occurrence outside protected areas by half during this period. Hence, our modeling results confirm the synergy between the two Ds of REDD (Reducing Emissions from Deforestation and Forest Degradation in Developing Countries). The loss of forest carbon to the atmosphere through fire represents a threat to the "permanence" of reductions in carbon emissions from deforestation and forest degradation through REDD programs. REDD will not compensate nations that reduce emissions from forest fire, but will penalize those nations whose reductions in emissions from deforestation are reversed through forest fire (Stickler et al. 2009). Comprehensive conservation strategies for the Amazon, therefore, require careful consideration of the interactions between climate change, deforestation, and fire.

Acknowledgments

The authors thank the Gordon and Betty Moore Foundation, the David and Lucille Packard Foundation, Conselho Nacional de Desenvolvimento Científico e Tecnológico–CNPQ, the Large-Scale Biosphere Atmosphere Experiment (LBA-ECO), and the AMAZONICA project for funding. We also gratefully acknowledge the contributions of Claudia Stickler and Maria Bowman for English language editing, two anonymous reviewers, whose comments improved the quality of the manuscript, Yosio Shimabukuro and Andre Lima for the forest-fire scar map, and Alberto Setzer for his suggestions.

Literature cited

Ackerman, A. S., O. B. Toon, D. E. Stevens, A. J. Heymsfield, V. Ramanathan, and E. J. Welton. 2000. Reduction of tropical cloudiness by soot. Science 288:1024–1047.

Agterberg, F. P., and G. F. Bonham-Carter. 1990. Deriving weights of evidence from geoscience contour maps for the prediction of discrete events. Pages 381–395 *in* XXII International Symposium. Volume 2. APCOM, Berlin, Germany.

Albini, F. A. 1996. Iterative solution of the radiation transport equations governing spread of fire in wildland fuel. Fizika Goreniya i Vzriva 32(5):71–82.

Alencar, A., D. C. Nepstad, and M. d. C. Vera Diaz. 2006. Forest understory fire in the Brazilian Amazon in ENSO and non ENSO years: area burned and committed carbon emissions. Earth Interactions 10:1–16.

Alencar, A. A. C., L. A. Solorzano, and D. C. Nepstad. 2004. Modeling forest understory fires in an eastern Amazonian landscape. Ecological Applications 14(Supplement):S139–S149.

Almeida, C., J. M. Gleriani, and E. F. Castejon. B. S. Soares Filho. 2008. Using neural networks and cellular automata for modeling intra-urban land use dynamics. International Journal of Geographical Information Science 22:943–963.

Andreae, M. O., D. Rosenfeld, P. Artaxo, A. A. Costa, G. P. Frank, K. M. Longo, and M. A. F. Silva-Dias. 2004. Smoking rain clouds over the Amazon. Science 303:1337–1342.

Aragão, L. E. O. C., Y. Malhi, R. M. Roman-Cuesta, S. Saatchi, L. O. Anderson, and Y. E. Shimabukuro. 2007. Spatial patterns and fire response of recent Amazonian droughts. Geophysical Research Letters 34:L07701.

Bailey, T., and T. Gatrell. 1995. Interactive spatial data analysis. Longman, New York, New York, USA.

Balch, J. K., D. C. Nepstad, and P. M. Brando. 2008. Negative fire feedback in a transitional forest of Southeastern Amazonia. Global Change Biology 14:1–12.

Bonham-Carter, G. 1994. Geographic information systems for geoscientists: modelling with GIS. Pergamon, Oxford, UK.

Botta, A., and J. A. Foley. 2002. Effects of climate variability and disturbances on the Amazonian terrestrial ecosystems dynamics. Global Biogeochemical Cycles 16:1070.

Brown, I. F., W. Schroeder, A. Setzer, M. d. L. R. Maldonado, N. Pantoja, A. Duarte, and J. A. Marengo. 2006. Monitoring fires in Southwestern Amazonia rain forests. EOS 87:253–264.

Butler, B. W., M. A. Finney, P. L. Andrews, and F. A. Albini. 2004. A radiation driven model for crown fire spread. Canadian Journal of Forest Research 34:1588–1599.

Cairns, M. A., W. M. Hao, E. Alvarado, and P. Haggerty. 2000. Crossing the millennium: integrating spatial technologies and ecological principles for a new age in fire management. Pages 242–247 *in* L. F. Neuenschwander, K. C. Ryan, G. E. Gollberg, and J. D. Greer. editors. Proceedings of the Joint Fire Science Conference and Workshop. Volume 1. University of Idaho and the International Association of Wildland Fire, Moscow, Idaho, USA.

Cândido, L. A., A. O. Manzi, J. Tota, P. R. T. da Silva, F. S. M. da Silva, R. N. N. dos Santos, and F. W. S. Correia. 2007. O clima atual e futuro da Amazônia nos cenários do IPCC: A questão da savanização. Ciência e Cultura 59(3):44–47.

Cardoso, M. F., C. G. Hurtt, B. Moore, C. A. Nobre, and E. M. Prins. 2003. Projecting future fire activity in Amazonia. Global Change Biology 9:656–669.

Carvalho, G., A. C. Barros, P. Moutinho, and D. Nepstad. 2001. Sensitive development could protect Amazonia instead of destroying it. Nature 409:131.

CFS [Canadian Forest Service]. 2007. Canadian forest fire danger rating system. Canadian Forest Service, Ottawa, Ontario, Canada. ⟨http://fire.cfs.nrcan.gc.ca/⟩

Chave, J., R. Condit, S. Aguilar, A. Hernandez, S. Lao, and R. Perez. 2004. Error propagation and scaling for tropical forest biomass estimates. Philosophical Transactions of the Royal Society B 359:409–420.

Cochrane, M. A. 2001. Synergistic interactions between habitat fragmentation and fire in evergreen tropical forests. Conservation Biology 15:1515–1521.

Cochrane, M. A. 2003. Fire science for rainforests. Nature 421:913–919.

Cochrane, M. A., and W. F. Laurance. 2002. Fire as a large-scale edge effect in Amazonian forests. Journal of Tropical Ecology 18:311–325.

Cochrane, M. A., et al. 1999. Positive feedbacks in the fire dynamic of closed canopy tropical forests. Science 284:1832–1835.

Collins, M. 2005. El Niño or La Niña climate change? Climate Dynamics 24:89–104.

Cox, P. M., R. A. Betts, C. B. Bunton, R. L. H. Essery, P. R. Rowntree, and J. Smith. 1999. The impact of new land surface physics on the GCM simulation of climate and sensitivity. Climate Dynamics 15:183–203.

Cox, P. M., R. A. Betts, M. Collins, P. P. Harris, C. Huntingford, and C. D. Jones. 2004. Amazonian forest dieback under climate-carbon cycle projections for the 21st century. Theoretical and Applied Climatology 78:137–156.

Cox, P. M., R. A. Betts, C. D. Jones, S. A. Spall, and I. J. Totterdell. 2000. Acceleration of global warming due to carbon-cycle feedbacks in a coupled climate model. Nature 408:184.

Cox, P., P. Harris, C. Huntingford, R. Betts, M. Collins, C. Jones, T. Jupp, J. Marengo, and C. Nobre. 2008. Increase risk of Amazonian drought due to decreasing aerosol pollution. Nature 453:212–216.

Cruz, G. C., M. E. Alexander, and R. H. Wakimoto. 2005. Developing and testing of models for predicting crown fire rate of spread in conifer forest stands. Canadian Journal of Forest Research 36:1626–1639.

Cruz, G. C., B. T. Butler, M. E. Alexander, J. M. Forthofer, and R. H. Wakmoto. 2006. Predicting the ignition of crown fuels above a spreading surface fire. Part I: model idealization. International Journal of Wildland Fire 15:47–60.

da Silva, R. R., D. Werth, and R. Avissar. 2008. Regional impacts of future land-cover changes on the Amazon Basin wet-season climate. Journal of Climate 21:1153–1170.

Delire, C., J. A. Foley, and S. Thompson. 2004. Long-term variability in a coupled atmosphere-biosphere model. Journal of Climate 17:3947–3959.

ESG [Earth System Grid II]. 2009. World Climate Research Programme's coupled model intercomparison Project Phase 3 (WCRP CMIP3) multi-model data. WCRP, Livermore, California, USA. ⟨https://esg.llnl.gov:8443/⟩

Fearnside, P. M. 1997. Greenhouse gases emissions from deforestation in Amazonia: net committed emissions. Climatic Change 35:321–360.

Gascon, C., G. B. Williamson, and G. A. B. Fonseca. 2000. Receding forest edges and vanishing reserves. Science 288:1356–1358.

Goldammer, J. G. 1990. Fire in the tropical biota. Pages 487–489 *in* Ecosystem processes and global challenges. Ecological Studies 84. Springer Verlag, Berlin, Germany.

Golding, N., and R. Betts. 2008. Fire risk in Amazonia due to climate change in the HadCM3 climate model: potential interactions with deforestation Global biogeochemical cycles 22:GB4007.

Gordon, C., et al. 2000. Simulation of SST, sea ice extents and ocean heat transport in a version of the Hadley Centre coupled model without flux adjustments. Climate Dynamics 16:147–168.

Haykin, S. S. 1999. Neural networks: a comprehensive foundation. Prentice-Hall, Upper Saddle River, New Jersey, USA.

Hirsch, A. I., W. S. Little, R. A. Houghton, N. A. Scott, and J. D. White. 2004. The net carbon flux due to deforestation and forest re-growth in the Brazilian Amazon: analysis using a process-based model. Global Change Biology 10:908–924.

Holdsworth, A. R., and C. Uhl. 1997. Fire in Amazonian selectively logged rain forest and the potential for fire reduction. Ecological Applications 7:713–725.

Houghton, R. A., K. T. Lawrence, J. Hackler, and L. S. Brown. 2001. The spatial distribution of forest biomass in the Brazilian Amazon: a comparison of estimates. Global Change Biology 7:731–746.

Houghton, R. A., D. L. Skole, C. A. Nobre, J. L. Hackler, K. T. Lawrence, and W. H. Chomentowski. 2000. Annual fluxes of carbon from deforestation and regrowth in the Brazilian Amazon. Nature 403:301–304.

Huete, A. K., et al. 2006. Amazon rainforests green-up with sunlight in dry season. Geophysical Research Letters 33:L06405.

IBGE [Instituto Brasileiro de Geografia e Estatística]. 2005. Base Cartográfica Integrada do Brasil ao Milionésimo Digital. Rio de Janeiro, Rio de Janeiro, Brazil. ⟨http://www.ibge.gov.br/home/geociencias/cartografia/default_territ_int.shtm?c=3⟩

INPE [Instituto Nacional de Pesquisas Espaciais]. 2008*a*. O Monitoramento de Queimadas em Tempo Quase-Real do INPE. Perguntas Freqüentes, São José dos Campos, São Paulo, Brazil. ⟨http://sigma.cptec.inpe.br/produto/queimadas/queimadas/perguntas.html⟩

INPE [Instituto Nacional de Pesquisas Espaciais]. 2008*b*. Projeto PRODES: Monitoramento da floresta Amazônica brasileira por satélite. Perguntas Freqüentes, São José dos Campos, São Paulo, Brazil. ⟨http://www.obt.inpe.br/prodes/⟩

IPCC. 2007. Climate change 2007: the physical science basis. Contribution of working Group I to the Fourth Assessment Report of the Intergovernmental Panel on Climate Change. Cambridge University Press, Cambridge, UK.

JRC [Joint Research Center]. 2009. Emissions database for global atmospheric research 4.0. JRC, Ispra, Varese, Italy. ⟨http://edgar.jrc.ec.europa.eu⟩

Kapos, V., G. Ganade, E. Matsui, and R. L. Victoria. 1993. $d^{13}C$ as an indicator of edge effects in tropical rainforest reserves. Journal of Ecology 81:425–431.

Koza, J. R. 1992. Genetic programming: on the programming of computer by means of natural selection—complex adaptive systems. MIT Press, Cambridge, Massachusetts, USA.

Kucharik, C. J., et al. 2000. Testing the performance of a dynamic global ecosystem model: water balance, carbon balance, and vegetation structure. Global Biogeochemical Cycles 14:795–825.

Laurance, W. F., S. G. Laurance, L. V. Ferreira, J. Ramkin-de Merona, C. Gascon, and T. E. Lovejoy. 1997. Biomass collapse in Amazonian forest fragments. Science 278:1117–1118.

Laurance, W. F., et al. 2001. The future of the Brazilian Amazon. Science 292:1651–1654.

Li, W., R. Fu, and R. E. Dickinson. 2006. Rainfall and its seasonality over the Amazon in the 21st century as assessed by the coupled models for the IPCC AR4. Journal of Geophysical Research 111:DO2111.

Lima, A., Y. E. Shimabukuro, M. Adami, R. M. Freitas, L. E. Aragão, A. R. Formaggio, and R. Lombardi. 2009. Mapeamento de cicatrizes de queimadas na Amazônia brasileira a partir da aplicação do modelo linear de mistura espectral em imagens do sensor MODIS. Pages 5925–5932 *in* Proceedings of XIV Simpósio Brasileiro de Sensoriamento Remoto. Natal, Rio Grande do Norte, Brazil.

Malhi, Y. J., T. Roberts, R. A. Betts, T. J. Killeen, W. Li, and C. A. Nobre. 2008. Climate change, deforestation and the fate of the Amazon. Science 319:169–172.

Malhi, Y. J., et al. 2009. Exploring the likelihood and mechanism of a climate-change-induced dieback of the Amazon rainforest. Proceedings of the National Academy of Sciences USA 106(49):20610.

Marengo, J. A., C. Nobre, J. Tomasella, M. Oyama, G. Sampaio, H. Camargo, and L. M. Alves. 2008. The drought of Amazônia in 2005. Journal of Climate 21:495–516.

Meggers, B. J. 1994. Archeological evidence for the impact of mega-Niño events on Amazonia during the past two millennia. Climate Change 28:321–338.

Mendonça, M. J. C., M. d. C. Vera Diaz, D. C. Daniel, R. Seroa, A. Alencar, J. C. Gomes, and R. A. Ortiz. 2004. The economic cost of the use of fire in the Brazilian Amazon. Ecological Economics 49:89–105.

Merry, F., B. S. Soares Filho, D. Nepstad, G. Amacher, and H. Rodrigues. 2009. Balancing conservation and economic sustainability: the future of the Amazon timber industry. Environmental Management 44:395–407.

Nepstad, D. C., A. G. Moreira, and A. Alencar. 1999*a*. Flames in the rain forest: origins, impacts and alternatives to Amazonian fire. The pilot program to conserve the Brazilian rain forest. World Bank, Brasilia, Distrito Federal, Brazil.

Nepstad, D. C., C. M. Stickler, and O. T. Almeida. 2006*a*. Globalization of the Amazon soy and beef industries: opportunities for conservation. Conservation Biology 20:1595–1603.

Nepstad, D., C. Stickler, B. S. Soares Filho, and F. Merry. 2008. Interactions among Amazon land use, forests, and climate: prospects for a near-term forest tipping point. Philosophical Transactions of the Royal Society B 363:1737–1746.

Nepstad, D. C., A. Verissimo, and A. Alencar. 1999*b*. Large-scale impoverishment of Amazonian forests by logging and fire. Nature 398:505–508.

Nepstad, D. C., et al. 2001. Road paving, fire regime feedbacks, and the future of Amazon forests Forest. Ecology and Management 154:395–407.

Nepstad, D. C., et al. 2004. Amazon drought and its implications for forest flammability and tree growth: a basin wide analysis. Global Change Biology 10:1–14.

Nepstad, D. C., et al. 2006*b*. Inhibition of Amazon deforestation and fire by parks and indigenous lands. Conservation Biology 20:65–73.

Nepstad, D. C., et al. 2009. The end of deforestation in the Brazilian Amazon. Science 326:1350–1351.

Nobre, C. A., P. J. Sellers, and J. Shukla. 1991. Amazonian deforestation and regional climate change. Journal of Climate 4:957–988.

NWCG [National Wildfire Coordinating Group]. 2002. Gaining an understanding of the National Fire Danger Rating System. NWCG, Boise, Idaho, USA. ⟨http://www.nwcg.gov/pms/pubs/MasterGaining.pdf⟩

Oyama, M. D., and C. A. Nobre. 2003. A new climate-vegetation equilibrium state for tropical South America. Geophysical Research Letters 30:23.

Page, S. S., F. Siegert, J. O. Rieley, H. V. Boehm, and A. Jaya. 2003. The amount of carbon released from peat and forest fires in Indonesia during 1997. Nature 420:61–65.

Phulpin, T., F. Lavenu, M. F. Bellan, B. Mougenot, and F. Blasco. 2002. Using SPOT-4 HRVIR and vegetation sensors to assess impact of tropical forest fires in Roraima, Brazil. International Journal of Remote Sensing 23:1943–1966.

Pontius, R. G., Jr., and L. Schneider. 2001. Land-use change model validation by a ROC method for the Ipswich watershed, Massachusetts, USA. Agriculture, Ecosystems and Environment 85:239–248.

Ramanathan, V., P. J. Crutzen, J. T. Kiehl, and D. Rosenfeld. 2001. Aerosols, climate and the hydrological cycle. Science 294:2119–2124.

Ray, D., D. Nepstad, and P. Moutinho. 2005. Micrometeorological and canopy controls of fire susceptibility in forested Amazon landscape. Ecological Applications 15:1664–1678.

Rothermel, R. C. 1972. A mathematical model for predicting fire spread in wildland fuels. Forest service General Technical Report INT-115. Intermountain Forest and Range Experiment Station, USDA Forest Service, Intermountain Forest and Range Experiment Station, Ogden, Utah, USA.

Saatchi, S. S., R. A. Houghton, A. R. C. dos Santos, Z. J. V. Soares, and Y. Yu. 2007. Distribution of aboveground live biomass in the Amazon basin. Global Change Biology 13:816–837.

Salazar, L. F., C. A. Nobre, and M. D. Oyama. 2007. Climate change consequences on the biome distribution in tropical South America. Geophysical Research Letters 34:L09708.

Sampaio, G., C. Nobre, M. H. Costa, P. Satyamurty, B. S. Soares-Filho, and M. Cardoso. 2007. Regional climate change over eastern Amazonia caused by pasture and soybean cropland expansion. Geophysical Research Letters 34(17):L17709.

Schroeder, W., J. Morissete, I. Csiszar, L. Giglio, D. Morton, and C. O. Justice. 2005. Characterizing vegetation fire dynamics in Brazil through multisatellite data: common trends and practical issues. Earth Interactions 9(13):1–26.

Sismanoglu, R. A., and A. W. Setzer. 2005. Risco de fogo da vegetação na América do Sul: comparação de três versões na estiagem de 2004. Pages 3349–3355 *in* Anais XII Simpósio Brasileiro de Sensoriamento Remoto. Goiânia, Goiás, Brazil.

Slik, J. W., R. W. Verburg, and P. J. A. Kebler. 2002. Effects of fire and selective logging on the tree species composition of lowland dipterocarp forest in East Kalimantan, Indonesia. Biodiversity and Conservation 11:85–98.

Soares-Filho, B., A. Alencar, D. Nepstad, G. C. Cerqueira, M. d. C. Vera Diaz, S. Rivero, L. Solórzano, and E. Voll. 2004. Simulating the response of land-cover changes to road paving and governance along a major Amazon highway: the Santarém-Cuiabá Corridor. Global Change Biology 10:745–764.

Soares-Filho, B. S., P. Moutinho, D. Nepsad, A. Anderson, H. Rodrigues, R. Garcia, L. Dietzsch, F. Merry, M. Bowman, L. Hissa, R. Silvestrini, and C. Maretti. 2010*a*. Role of Brazilian Amazon protected areas in climate change mitigation. Proceedings of the National Academy of Sciences USA 107:10821–10826.

Soares-Filho, B. S., H. O. Rodrigues, and W. L. Costa. 2010*b*. Modeling environmental dynamics with Dinamica EGO. Belo Horizonte, Minas Gerais, Brazil. ⟨http://www.csr.ufmg.br/dinamica⟩

Soares-Filho, B. S., et al. 2006. Modelling conservation in the Amazon basin. Nature 440:520-523.

Stickler, C. M., et al. 2009. The potential ecological costs and co-benefits of REDD: a critical review and case study from the Amazon region. Global Change Biology 15:2803–2824.

Uhl, C., and J. B. Kauffman. 1990. Deforestation, fire susceptibility, and potential tree responses to fire in the eastern Amazon. Ecology 71:437–449.

van der Werf, G. R., et al. 2009. CO_2 emissions from forest loss. Nature Geoscience 2:737–738.

Venevsky, S., K. Thonicke, S. Sitch, and W. Cramer. 2002. Simulating fire regimes in human-dominated ecosystems: Iberian Peninsula case study. Global Change Biology 8:984–998.

Xiao, X., S. Hagen, Q. Zhang, M. Keller, and B. Moore. 2006. Detecting leaf phenology of seasonally moist tropical forests in South America with multi-temporal MODIS images. Remote Sensing of Environment 103:465–473.

Xiao, X., et al. 2005. Satellite-based modeling of gross primary production in a seasonally moist tropical evergreen forest. Remote Sensing of Environment 94:105–122.